Figure 2 shows the temperature distribution of the battery with four different channel designs. The four channel designs have little effect on the maximum temperature difference of the battery. The maximum temperature of the battery in the transverse symmetric serpentine channel, longitudinal symmetric serpentine channel, parallel double serpentine channel, and parallel triple serpentine channel are 36.05, 35.72, 35.98, and 36.07 ℃, respectively.

However, the temperature distribution characteristics of the four types of battery designs are slightly different. For the transverse symmetric serpentine flow channel and the longitudinal symmetric serpentine flow channel, the battery temperature is relatively low in the coolant inlet area, while the battery temperature is relatively high in the coolant outlet area. Due to continuous heat absorption, the coolant temperature continues to rise along the flow path, resulting in poorer heat dissipation along the coolant flow path. For parallel double serpentine flow channels and parallel triple serpentine flow channels, due to the fact that the coolant inlet and outlet are located on the same side, the heat exchange between the low temperature zone at the coolant inlet and the high temperature zone at the outlet is strengthened, thereby increasing the minimum temperature of the battery and reducing the maximum temperature difference of the battery. The maximum temperature difference of the battery for four designs: transverse symmetric serpentine flow channel, longitudinal symmetric serpentine flow channel, parallel double serpentine flow channel, and parallel triple serpentine flow channel is 4.17 ℃, 3.65 ℃, 2.83 ℃, and 3.42 ℃.

Literature:

B Nykvist, M Nilsson. Rapidly falling costs of battery packs for electric vehicles[J]. Nature Climate Change, 2015, 5(4):329-332.

M Fleischhammer, T Waldmann, G Bisle, et al. Interaction of cyclic ageing at high-rate and low temperatures and safety in lithium-ion batteries[J]. Journal of Power Sources, 2015, 274(1):432-439.

W Zuo, Y Zhang, J E, et al. Performance comparison between single S-channel and double S-channel cold plate for thermal management of a prismatic LiFePO4 battery[J]. Renewable Energy, 2022, 192(1):46-57.

THE TRANSIENT THERMAL STRESS DISTRIBUTING BEHAVIOR WITHIN A TYPICAL SOFC STACK DURING THE PREHEATING PROCESS

Yanlong Zhu[1], Shuo Han[1], Zhe Zhang[1], Changchun Xu[1,*], Serhiy Serbin[2], Daifen Chen[1,*]

1 School of Energy and Power, Jiangsu University of Science and Technology, Zhenjiang 212100, China

2. Department of Turbine Units, National University of Shipbuilding, Heroes of Ukraine Ave. 9, 54025 Mykolaiv, Ukraine

**Corresponding authors. 202200000004@just.edu.cn (C. Xu), dfchen@just.edu.cn (D. Chen)*

Summary

Mechanical stability and integrity are essential prerequisites for achieving long term stability and maintaining high performance of solid oxide fuel cell (SOFC) stack, especially at the preheating stage. In this study, a transient 3D thermomechanical model basing on the realistic component structure is firstly developed for investigating the evolution of the transient thermal stress distribution with the running time during the preheating process. Then, the effects of different interconnector structures on the thermodynamic distributing characteristics within a typical SOFC stack at the preheating stages are analyzed. The coupling calculated results show that compared with the interconnector plate with rectangular ribs, using the cylindrical

ribs for the anode and cathode sides can reduce the thermal stresses by 13% and 25%, respectively. The first principal stress of the electrolyte will be significantly affected by the interconnector structure features. Adopting the cylindrical ribs can reduce the first principal stress of the electrolyte by 150 MPa at 5400 s and keep it within the range of 20 MPa for all the preheating and working processes.

Keywords: Solid oxide fuel cell stack, Variation of Transient thermal stress, Calculated fluid dynamics, Calculated solid mechanics, Thermo-mechanic simulation.

Text

As fossil electricity reserves are being depleted and environmental air pollution worsens, innovating power utilization technological and looking out for alternative fuels have turned out to be two important challenges[1-4]. Solid oxide fuel cells convert chemical energy of fuels directly into electricity with low loss and emission[5, 6]. Compared to the traditional thermal electricity plants, SOFC has won growing interests due to its a couple of distinguish advantages. These make it a promising technological know-how for attaining environment-friendly electricity utilization and assembly carbon neutrality dream[7-10].

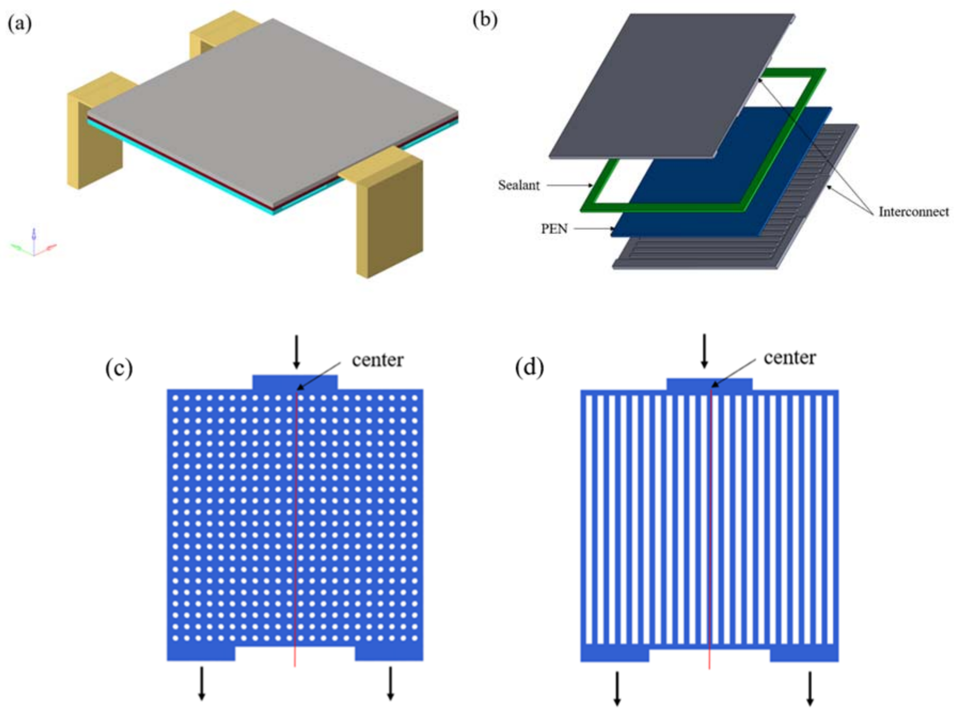

Figure 1 a) 3D model of a typical SOFC stack with one cell unit; b) the components of each SOFC unit including interconnect, sealant, and PEN (anode, electrolyte, and cathode layers); c) cylindrical ribs; d) rectangular ribs.

As shown in **Fig. 1a**, we established a transient three-dimensional thermodynamic model of the actual component structure to study the rule of time change of the thermal stress of a single-layer electric reactor with a typical structure of a 3D model solid oxide fuel cell. As shown in **Fig. 1b**, the components of each SOFC unit in the 3D model are composed of an interconnect layer, a sealant layer, and a PEN layer. The PEN layer comprises an anode layer, an electrolyte layer and a cathode layer. We further coupled the cylindrical structure reactor to verify the effectiveness of the constructed transient three-dimensional thermal stress model in dealing with complex reactors, including the temperature distribution with time (I), the equivalent stress distribution with time (II), and the maximum principal stress distribution with time (III).

a) Rectangular ribs (I) **b）Cylindrical ribs (I)**

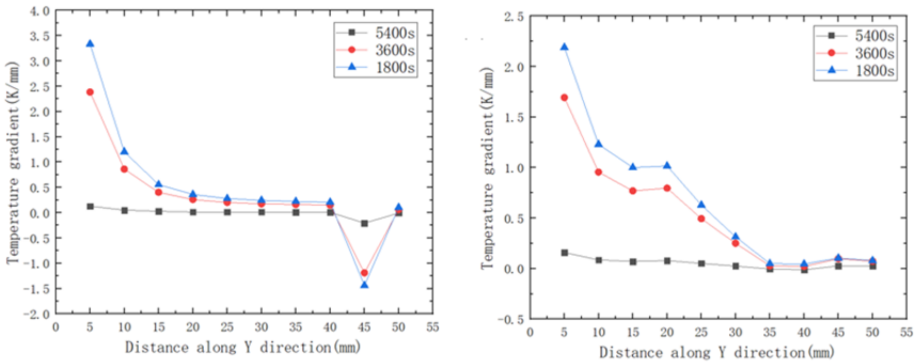

Figure 2 The temperature gradient of electrolyte in the preheating stage,
a）Rectangular ribs, b）Cylindrical ribs

2) The temperature distribution with time (I) in ***Fig.2,*** *consists of the* typical rectangular rib shown in **Fig. 2a** and the typical cylindrical rib shown in **Fig. 2b** based on the 3D transient thermal stress model study.

a) Since the cathode is used for heating the SOFC by passing hot air, as shown in **Fig. 2**, the temperature rises faster at the air inlet. Meanwhile, the temperature rises slower in other parts of the cell that are farther from the air inlet. Moreover, the temperature gradually decreases along the airflow direction.

b) It was observed that the cell temperature rises at a slower rate as time progresses. This means that at the beginning of the heating phase, the cell temperature undergoes faster changes and has a larger temperature gradient, but as heating continues, the temperature changes become slower and the temperature gradient gradually decreases. In terms of the rectangular and cylindrical ribs shown in **Fig. 2a** and **2b** respectively, the direction and trend of temperature transfer are consistent.

c) As depicted in **Fig. 2**, the largest temperature gradient at the cathode side inlet position is observed when heating reaches the 1800s, with the cylindrical rib exhibiting a gradient of 2.5 K/mm and the rectangular rib showing a gradient of 3.47 K/mm. As heating progresses to 5400s, the temperature gradient of both types of cells becomes very small and relatively uniform, with the cylindrical rib having the highest value at 0.15 K/mm and the lowest at -0.003 K/mm, while the rectangular rib has the highest at 0.12 K/mm and the lowest at -0.2 K/mm. This is because in the initial stage of preheating, convective heat transfer plays a dominant role in the temperature transfer process, and each flow channel of the rectangular rib is independent of each other, and the heat mainly relies on the heating of the IC at the inlet position to achieve preheating of the cell, with poor heat transfer effect and large temperature gradient. The rectangular rib (**Fig. 2a**) has a temperature gradient interval of the electrolyte is 4.94 K/mm. The cylindrical rid flow channels are connected, and the high-temperature air can fill each position of the cell in a short time, transforming the local heating into the overall heating, and achieving uniformity of temperature. The temperature gradient interval of the electrolyte in the cylindrical rib (**Fig. 2b**) is 2.503 K/mm.

3) The equivalent stress distribution with time (II), is shown in **Fig. 3a** and **Fig. 3b,** respectively. The model we constructed shows that the equivalent stress of IC is greatly affected by its shape, and this influence does not change with time. The distribution trends of the IC equivalent stresses on the anode and cathode sides are similar. The large stresses are commonly determined at the edges and sharp corners of the ribs and alongside the periphery of the ribs, where the coexistence of material discontinuities, geometric discontinuities, and large temperature gradients leads to greater thermal stresses. The periphery of the ribs in areas close to the inlet or outlet is more susceptible to thermal stresses than the middle part of the ribs, which experiences lower thermal stresses than the surrounding ribs. The tendency of the distribution of these effect stresses does not change with increasing preheating time. As the temperature increases, the stress-prone areas in the rounded areas and at the ribs decrease with time and remain at lower values. Therefore, special attention needs to be paid to the initial stage of the heating process, where the components are subjected to the highest thermo-mechanical loads and require careful control.

Anode side (II) Cathode side (II)

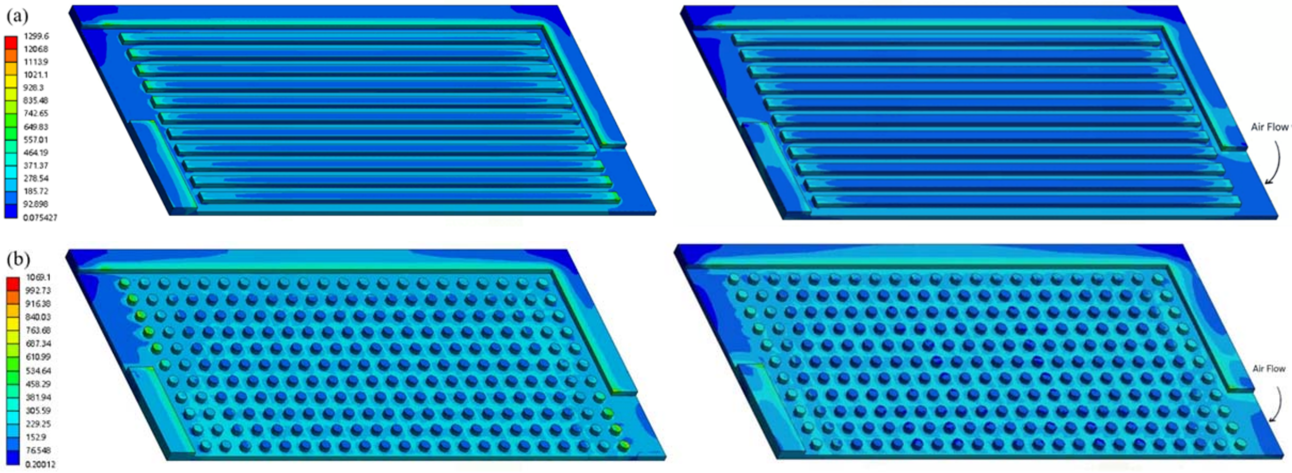

Figure 3 Equivalent stress (MPa) of IC on the anode side (left) and cathode side (right) during the preheating stage, a) rectangular rib, b) cylindrical rib.

Anode side (III) Cathode side (III)

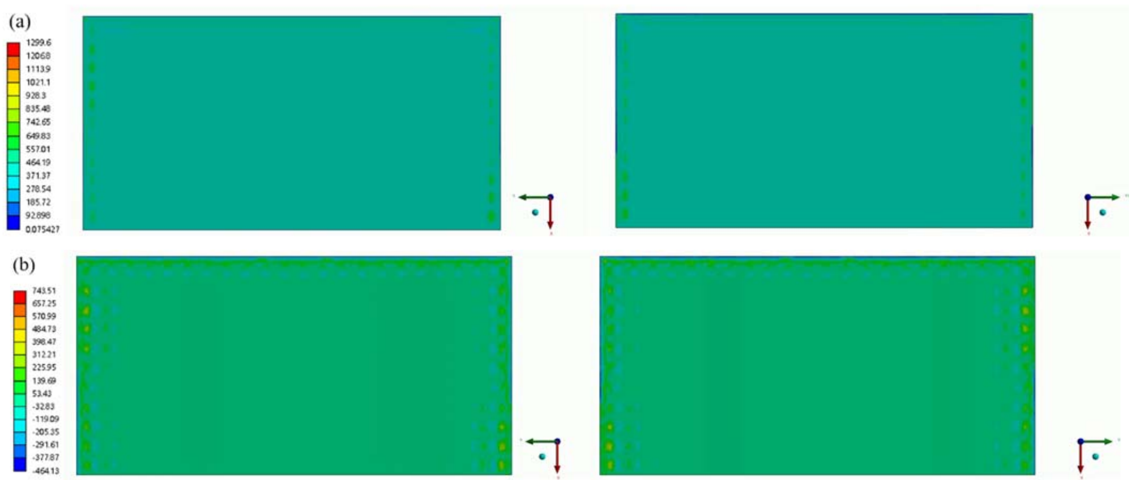

Figure 4 First principal stress distribution (MPa) of the electrolyte at the anode side (left) and cathode side (right) during the preheating stage, a) rectangular rib, b) cylindrical rib

4) the maximum principal stress distribution with time (III) is shown in **Fig. 4a** and **Fig. 4b,** respectively. Although the first principal stress of the electrolyte does not change significantly during the preheating stage, compared to **Fig. 4b**, the thermal stresses in the electrolyte proven in **Fig. 4a** are influenced by the IC design. The alternating association of ribs and channels consequences in an attributed spatially periodic distribution of thermal stresses in the electrolyte due to the fact the electrolyte below the channels has greater freedom of deformation, while the electrolyte under the ribs is constrained. Tensile stresses are located in the region under the ribs, while the region under the channels is subjected to relatively small tensile stresses or even compressible stress. As the preheating time increases, the periodic distribution characteristic weakens, and the first principal stresses at the inlet and outlet positions start to decrease, while the first principal stresses in the intermediate region continue to increase. In contrast, in **Fig. 4b**, the first principal stress of the electrolyte on both the anode and cathode sides remains very low, which is very different from the first principal stress of the rectangular rib in **Fig. 4a**. This is because the rectangular ribs are rounded and the single ribs are interrupted to become dispersed rectangular ribs, so that the force borne by the electrolyte is uniform and dispersed, and the possible delamination phenomenon in the middle of the electrolyte is avoided. During the preheating stage, the greater thermal stress produced by the electrolytes can be dispersed to lower-stress locations, thus transforming the thermal stress from a point concentration to a plane distribution and maintaining lower stress. However, it can still be predicted that there is still a risk of fracture at the interface between the rectangular rib electrolyte and the anode.

Interestingly, the transient three-dimensional thermodynamic model established by us can be used to observe the trend of thermal stress variation over time in the preheating stage of solid oxide fuel cells, and further analyze the more complex cylindrical structures, and study the influence of different structures on the thermal stress distribution over time in the preheating stage in detail.

Literature：

[1].Fu, Q.R., Z.Y. Li, W. Wei, F.X. Liu, X.F. Xu, and Z.J. Liu, Performance enhancement of a beam and slot interconnector for anode-supported SOFC stack. Energy Conversion and Management, 241(2021),114277.

[2].Li, Y., Q.L. Zhou, J.T. Wu, J.H. Xu, W.L. Shi, C. Su, D.F. Chen, and Z.P. Shao, Controllably grown single-crystal films as flexoelectric nanogenerators for continuous direct current output. Npj Flexible Electronics, 6(2022), 88.

[3].Shi, H., C. Su, R. Ran, J. Cao, and Z. Shao, Electrolyte materials for intermediate-temperature solid oxide fuel cells. Progress in Natural Science: Materials International, 2020. 30(6): p. 764-774.

[4].Wei, T., J.H. Lu, M.T. Wang, C. Sun, Q. Zhang, S.J. Wang, Y.Y. Zhou, D.F. Chen, and Y.Q. Lan, MOF-Derived Materials Enabled Lithiophilic 3D Hosts for Lithium Metal Anode - A Review. Chinese Journal of Chemistry, 2023. https://doi.org/10.1002/cjoc.202200816

[5].Fang, X.R. and Z.J. Lin, Numerical study on the mechanical stress and mechanical failure of planar solid oxide fuel cell. Applied Energy, 2018. 229: p. 63-68.

[6].Zhang, H., H. Qin, W. Zhao, J. Jiang, X. Li, and J. Li, Thermoelectrical-based fuel adaptability analysis of solid oxide fuel cell system and fuel conversion rate prediction. Energy Conversion and Management, 222(2020), 113264.

[7].Chen, D.F., Q.C. Zeng, S.C. Su, W.X. Bi, and Z.Q. Ren, Geometric optimization of a 10-cell modular planar solid oxide fuel cell stack manifold. Applied Energy, 2013. 112: p. 1100-1107.

[8].Hu, C., Y. Zhao, Z. Zhang, H.Y. Zhang, and D.F. Chen, Optimization of flow field structure for proton exchange membrane fuel cell stack by multi-physics coupling simulation. International Journal of Electrochemical Science, 2023. 18(7).

[9].Huang, Q., S.S. Jiang, Y.J. Wang, J.J. Jiang, Y.B. Chen, J.H. Xu, H. Qiu, C. Su, and D.F. Chen, Highly active and durable triple conducting composite air electrode for low-temperature protonic ceramic fuel cells. Nano Research, 2023. https://doi.org/10.1007/s12274-023-5531-3

[10].Park, S.K., T.S. Kim, J.L. Sohn, and Y.D. Lee, An integrated power generation system combining solid oxide fuel cell and oxy-fuel combustion for high performance and CO2 capture. Applied Energy, 2011. 88(4): p. 1187-1196.